6th European Conference on Computational Mechanics (ECCM 6)
7th European Conference on Computational Fluid Dynamics (ECFD 7)
1115 June 2018, Glasgow, UK

POD-DEIM MODEL ORDER REDUCTION FOR THE MONODOMAIN REACTION-DIFFUSION EQUATION IN NEURO-MUSCULAR SYSTEM

N. EMAMY*[,1], P. LITTY[1], T. KLOTZ[2], M. MEHL[1] and O. RÖHRLE[2]

[1] Institute for Parallel and Distributed Systems, University of Stuttgart, Universitätstr. 38, 70569 Stuttgart, Germany [nehzat.emamy,miriam.mehl]@ipvs.uni-stuttgart.de, https://www.ipvs.uni-stuttgart.de/abteilungen/sgs/

[2] Institute of Applied Mechanics (CE), SimTech Research Group on Continuum Biomechanics and Mechanobiology, University of Stuttgart Pfaffenwaldring 5a, 70569 Stuttgart, Germany thomas.klotz@mechbau.uni-stuttgart.de, roehrle@simtech.uni-stuttgart.de, http://www.mechbau.uni-stuttgart.de/ls2/jrg/index.html

Key words: Model order reduction, Neuro-muscular system, Coupled problems, Multi-scale, Reaction-diffusion, POD, DEIM

Abstract. We apply the POD-DEIM model order reduction to the propagation of the transmembrane potential along 1D muscle fibers. This propagation is represented using the monodomain partial differential equation. The monodomain equation, which is a reaction-diffusion equation, is coupled through its reaction term with a set of ordinary differential equations, which provide the ionic current across the cell membrane. Due to the strong coupling of the transmembrane potential and ionic state variables, we reduce them all together proposing a total reduction strategy. We compare the current strategy with the conventional strategy of reducing the transmembrane potential. Considering the current approach, the discrete system matrix is slightly modified to adjust for the size. However, size of the precomputed reduced system matrix remains the same, which means the same computational cost. The current approach appears to be four orders of magnitude more accurate considering the equivalent number of modes on the same grid in comparison to the conventional approach. Moreover, it shows a faster convergence in the number of POD modes with respect to the grid refinement. Using the DEIM approximation of nonlinear functions in combination with the total reduction, the nonlinear functions corresponding to the ionic state variables are also approximated besides the nonlinear ionic current in the monodomain equation. For the current POD-DEIM approach, it appears that the same number of DEIM interpolation points as the number of POD modes is the optimal choice regarding stability, accuracy and runtime.

1 Introduction

The neuro-muscular system is a complex multiscale coupled system, for which chemo-electromechanical models are proposed as e.g. in [1, 2, 3]. Realistic simulations of such

models are computationally extremely demanding. One challenging part of the model is the partial differential equation (PDE) describing the propagation of the transmembrane potentials along muscle fibers. The PDE is coupled with a set of nonlinear ordinary differential equations (ODEs), which resemble ionic currents at the cell membrane. To reduce the computational costs, one could apply model order reduction techniques. For spiking neurons, the model order reduction is applied in [4], where the proper orthogonal decomposition (POD) is used together with the proposed discrete empirical interpolation method (DEIM) to approximate the nonlinear ionic current resulting from the Hodgkin and Huxley (1952) model [5]. For parameter identification in cardiac electrophysiology, the POD approach is used to build a reduced basis for the extracellular and transmembrane potentials [6]. The POD-DEIM approach is used in [7] to estimate the cardiac conductivities and in [8] to study electromyographic signals for skeletal muscles.
The usual reduction approach as used in the above mentioned studies, is to consider snapshots of the transmembrane potential and nonlinear ionic current to build the POD bases. However, as the transmembrane potential and ionic state variables are strongly coupled, we focus on a reduction strategy to reduce them all together. We call this strategy and the usual approach as total and partial reduction strategies, respectively, which we introduce in section 4. In sections 2 and 3, we show the monodomain equation and its discrete version, respectively. The introduced partial and total reduction strategies are compared in section 5 for the POD approach. The POD-DEIM approach using the total reduction is studied in section 6.

2 Propagation of the transmembrane potentials along muscle fibers

Considering skeletal muscles, the propagation of transmembrane potentials along muscle fibers are well approximated as 1D problems using the monodomain equation. The monodomain equation comprises the diffusion of the transmembrane potentials along 1D muscle fibers in domain $\Gamma \subset \mathbb{R}$ and the microscopic reactions existing at the cell membrane,

$$\frac{\partial V_\mathrm{m}}{\partial t} = \frac{1}{A_\mathrm{m} C_\mathrm{m}} \left(\frac{\partial}{\partial x} \Big(\sigma_\mathrm{eff} \frac{\partial V_\mathrm{m}}{\partial x} \Big) - A_\mathrm{m} I_\mathrm{ion}\big(\boldsymbol{y}, V_\mathrm{m}, I_\mathrm{stim}\big) \right) \text{ in } \Gamma, \tag{1a}$$

$$\frac{\partial \boldsymbol{y}}{\partial t} = G\left(\boldsymbol{y}, V_\mathrm{m}\right), \tag{1b}$$

where V_m is the transmembrane (action) potential, C_m is the capacitance of the muscle fiber transmembrane (sarcolemma), A_m is the fiber's surface to volume ratio and σ_eff is the effective conductivity. x denotes the spatial coordinate along the fiber. I_ion is the ionic current flowing over the ion-channels and -pumps. Further state variables are summarized in $\boldsymbol{y}$, e. g. the states of different ion-channels, which depend on V_m, as well. I_stim is an externally applied stimulation current due to a stimulus from the nervous system. G summarizes the right-hand-side of all nonlinear ODEs associated with the state variables $\boldsymbol{y}$. Here, we consider the biophysically motivated model of Hodgkin and Huxley (1952) [5], which is the base model to describe the ionic mechanism in the cell membrane. For this model, $\boldsymbol{y} \in \mathbb{R}^3$ represent the three gating variables related to activation/inactivation

of potassium and sodium ion-channels. We apply homogeneous Neumann boundary conditions for V_m at both ends of the 1 cm long fiber. The initial values for V_m and $\boldsymbol{y}$ are set according to the Hodgkin and Huxley model. The stimulation current is applied at the middle of the fiber.

3 Discrete system

For the time integration of the monodomain equation (1a), we apply the Godunov splitting scheme, where we integrate the reaction and diffusion terms in two steps. The reaction term is integrated together with (1b) using the explicit Euler scheme and the diffusion terms is integrated using the implicit Euler scheme.

$$\begin{bmatrix} V_\mathrm{m}^* \\ \boldsymbol{y}^{(n+1)} \end{bmatrix} = \begin{bmatrix} V_\mathrm{m}^{(n)} \\ \boldsymbol{y}^{(n)} \end{bmatrix} + dt \begin{bmatrix} -\frac{1}{C_\mathrm{m}} I_\mathrm{ion}\big(V_\mathrm{m}^{(n)}, \boldsymbol{y}^{(n)}, I_\mathrm{stim}^{(n)}\big) \\ G\big(V_\mathrm{m}^{(n)}, \boldsymbol{y}^{(n)}\big) \end{bmatrix}, \tag{2a}$$

$$V_\mathrm{m}^{(n+1)} = V_\mathrm{m}^* + \frac{dt}{A_\mathrm{m} C_\mathrm{m}} \frac{\partial}{\partial x}\Big(\sigma_\mathrm{eff} \frac{\partial V_\mathrm{m}^{(n+1)}}{\partial x}\Big) \quad \text{in } \Gamma \tag{2b}$$

V_m^* denotes an intermediate transmembrane potential. After the spatial discretization using the FEM method, we have the following discrete system of equations, which define our full order model,

$$\begin{bmatrix} \mathbf{v}_\mathrm{m}^* \\ \mathbf{y}^{(n+1)} \end{bmatrix} = \begin{bmatrix} \mathbf{v}_\mathrm{m}^{(n)} \\ \mathbf{y}^{(n)} \end{bmatrix} + \begin{bmatrix} \mathbf{F}(\mathbf{v}_\mathrm{m}^{(n)}, \mathbf{y}^{(n)}) + \mathbf{B}\mathbf{u}^{(n)} \\ \mathbf{G}(\mathbf{v}_\mathrm{m}^{(n)}, \mathbf{y}^{(n)}) \end{bmatrix}, \tag{3a}$$

$$\mathbf{v}_\mathrm{m}^{(n+1)} = \mathbf{v}_\mathrm{m}^* + \mathbf{A}\mathbf{v}_\mathrm{m}^{(n+1)}, \tag{3b}$$

where $\mathbf{v}_\mathrm{m}$, $\mathbf{Bu} \in \mathbb{R}^n$ and $\mathbf{A} \in \mathbb{R}^{n\times n}$. $\mathbf{y} \in \mathbb{R}^{3n}$, $\mathbf{F} : \mathcal{I} \mapsto \mathbb{R}^n$ and $\mathbf{G} : \mathcal{I} \mapsto \mathbb{R}^{3n}$ for $\mathcal{I} \subset \mathbb{R}^{4n}$. $\mathbf{Bu}$ implements the stimulation current as an input term, which is adjustable linearly with the number of nodes in the grid.

4 Reduction strategy

To study the potential for model order reduction, the singular value decomposition (SVD) is applied on the snapshot (sample of trajectory) matrix $\mathbf{S} = [\mathbf{s}_1, ..., \mathbf{s}_{n_s}]$,

$$\mathbf{S} = \mathbf{V}\mathbf{\Sigma}\mathbf{W}^\mathrm{T}.$$

Here we follow the notation in [9], where $\mathbf{\Sigma} = \mathrm{diag}(\sigma_1, ..., \sigma_r) \in \mathbb{R}^{r\times r}$, with $\sigma_1 \geq \sigma_2 \geq ... \geq \sigma_r > 0$. The rank of $\mathbf{S}$ is $r \leq \min(n, n_s)$. n_s is the number of snapshots. The snapshots are gathered every time step 0.0005 ms for 10 ms ($n_s = 20000$) for grids of $n = 10, 20, 40, 80, 160$ and 320 nodes. We consider two strategies with respect to the snapshots. First, for a partial reduction, we choose the snapshots of the transmembrane

potential to have the snapshot matrix,

$$\mathbf{S}_{n\times n_s} = \begin{bmatrix} {v_{\mathrm{m}}}_1^1 & {v_{\mathrm{m}}}_1^2 & \dots & {v_{\mathrm{m}}}_1^{n_s} \\ \vdots & \vdots & \dots & \vdots \\ {v_{\mathrm{m}}}_n^1 & {v_{\mathrm{m}}}_n^2 & \dots & {v_{\mathrm{m}}}_n^{n_s} \end{bmatrix}.$$

Second, for a total reduction, we consider the snapshots of the transmembrane potential and the three state variables,

$$\mathbf{S}_{4n\times n_s} = \begin{bmatrix} {v_{\mathrm{m}}}_1^1 & {v_{\mathrm{m}}}_1^2 & \dots & {v_{\mathrm{m}}}_1^{n_s} \\ {y_1}_1^1 & {y_1}_1^2 & \dots & {y_1}_1^{n_s} \\ {y_2}_1^1 & {y_2}_1^2 & \dots & {y_2}_1^{n_s} \\ {y_3}_1^1 & {y_3}_1^2 & \dots & {y_3}_1^{n_s} \\ \vdots & \vdots & \dots & \vdots \\ {v_{\mathrm{m}}}_n^1 & {v_{\mathrm{m}}}_n^2 & \dots & {v_{\mathrm{m}}}_n^{n_s} \\ {y_1}_n^1 & {y_1}_n^2 & \dots & {y_1}_n^{n_s} \\ {y_2}_n^1 & {y_2}_n^2 & \dots & {y_2}_n^{n_s} \\ {y_3}_n^1 & {y_3}_n^2 & \dots & {y_3}_n^{n_s} \end{bmatrix}.$$

Note that $\mathbf{V}$, which contains the left singular vectors of $\mathbf{S}$, has the dimensions $n \times r$ and $4n \times r$ considering the partial and total reduction strategies, respectively. The singular values are shown in Figures 1 and 2 for the two strategies. There are jumps in the singular values, at which one can set a threshold for the reduction. A convergence with respect to grid refinement could be observed for both strategies. We consider a threshold of 10^{-5} for the singular values and show the number of singular values, which are greater than this threshold in Table 1. Number of the modes k shows to converge by grid refinement for both strategies. The k/r ratio shows the ratio of the modes corresponding to the transmembrane potential for both strategies. The small ratios show that the reduction is more effective using fine grids. Using the total reduction, a faster convergence in k by the grid refinement and much smaller ratios k/r on the same grid are achieved in comparison to the partial reduction.

Table 1: Comparison of the singular values considering the partial and total reduction strategies for different grids. k/r shows the ratio of the number of singular values greater than 10^{-5} to the rank of snapshot matrix.

	Partial reduction						Total reduction					
n	10	20	40	80	160	320	10	20	40	80	160	320
r	10	20	40	80	160	320	40	80	160	320	640	1280
k	8	18	38	78	120	124	32	72	121	135	157	160
k/r	0.8	0.9	0.95	0.98	0.75	0.39	0.8	0.9	0.76	0.42	0.245	0.16

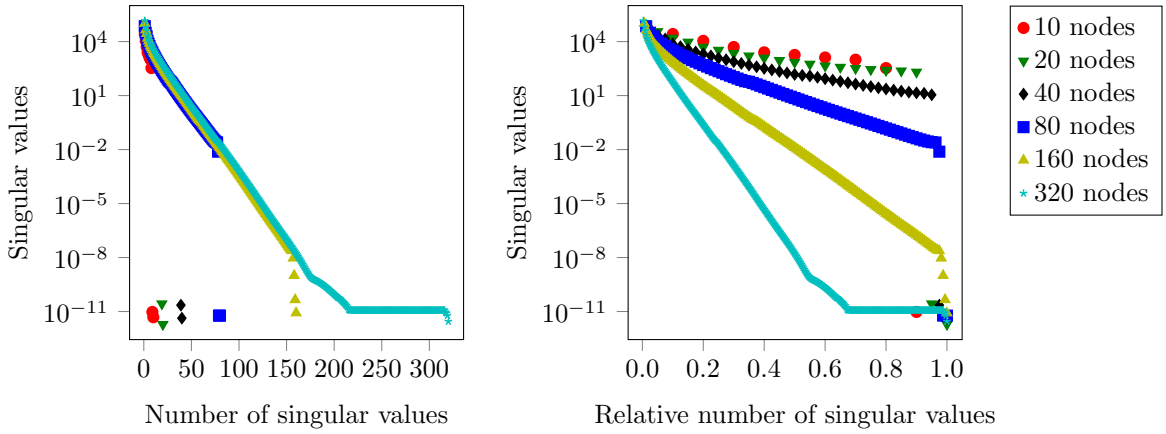

Figure 1: Singular value decomposition of the snapshot matrix containing the transmembrane potentials using the partial reduction strategy.

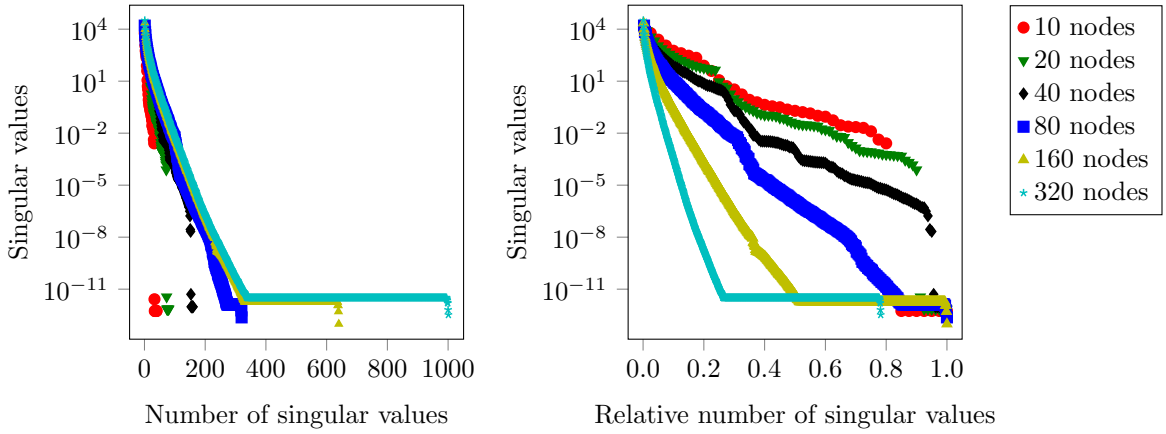

Figure 2: Singular value decomposition of the snapshot matrix containing the transmembrane potential and three ion-channel state variables using the total reduction strategy.

5 POD-Galerkin approach

The set of left singular vectors of the snapshot matrix provides the basis for the POD approximation of the snapshots, where the minimum L2-norm error of the approximation is given by

$$\sum_{j=1}^{n_s} \left|\left| \mathbf{s}_j - \sum_{i=1}^{k} (\mathbf{s}_j^{\mathrm{T}} \mathbf{v}_i) \mathbf{v}_i \right|\right|_2^2 = \sum_{i=k+1}^{r} \sigma_i^2. \tag{4}$$

We use the KerMor[1] [10] library and apply the Galerkin projection of the system (3) above. Using the partial reduction, we have the following reduced system to solve,

$$\begin{bmatrix} \tilde{\mathbf{v}}_{\mathrm{m}}^{*} \\ \mathbf{y}^{(n+1)} \end{bmatrix} = \begin{bmatrix} \tilde{\mathbf{v}}_{\mathrm{m}}^{(n)} \\ \mathbf{y}^{(n)} \end{bmatrix} + \begin{bmatrix} \mathbf{V}_k^{\mathrm{T}}\mathbf{F}(\mathbf{v}_{\mathrm{m}}^{(n)}, \mathbf{y}^{(n)}) + \mathbf{V}_k^{\mathrm{T}}\mathbf{B}\mathbf{u}^{(n)} \\ \mathbf{G}(\mathbf{v}_{\mathrm{m}}^{(n)}, \mathbf{y}^{(n)}) \end{bmatrix}, \tag{5a}$$

$$\tilde{\mathbf{v}}_{\mathrm{m}}^{(n+1)} = \tilde{\mathbf{v}}_{\mathrm{m}}^{*} + \mathbf{V}_k^{\mathrm{T}}\mathbf{A}\mathbf{V}_k\tilde{\mathbf{v}}_{\mathrm{m}}^{(n+1)}, \tag{5b}$$

where $\mathbf{v}_{\mathrm{m}} = \mathbf{V}_k\tilde{\mathbf{v}}_{\mathrm{m}}$. The reduced transmembrane potential $\tilde{\mathbf{v}}_{\mathrm{m}} \in \mathbb{R}^k$ and $\mathbf{V}_k$ is the matrix of k left singular vectors of the snapshot matrix with $k < r$. Considering the total reduction, we have

$$\begin{bmatrix} \tilde{\mathbf{v}}_{\mathrm{m}}^{*} \\ \tilde{\mathbf{y}}^{(n+1)} \end{bmatrix} = \begin{bmatrix} \tilde{\mathbf{v}}_{\mathrm{m}}^{(n)} \\ \tilde{\mathbf{y}}^{(n)} \end{bmatrix} + \mathbf{V}_k^{\mathrm{T}} \begin{bmatrix} \mathbf{F}(\mathbf{v}_{\mathrm{m}}^{(n)}, \mathbf{y}^{(n)}) \\ \mathbf{G}(\mathbf{v}_{\mathrm{m}}^{(n)}, \mathbf{y}^{(n)}) \end{bmatrix} + \mathbf{V}_k^{\mathrm{T}}\mathbf{B}\mathbf{u}^{(n)}, \tag{6a}$$

$$\tilde{\mathbf{v}}_{\mathrm{m}}^{(n+1)} = \tilde{\mathbf{v}}_{\mathrm{m}}^{*} + \mathbf{V}_k^{\mathrm{T}}\mathbf{A}\mathbf{V}_k\tilde{\mathbf{v}}_{\mathrm{m}}^{(n+1)}, \tag{6b}$$

where $\begin{bmatrix} \mathbf{v}_{\mathrm{m}} \\ \mathbf{y} \end{bmatrix} = \mathbf{V}_k \begin{bmatrix} \tilde{\mathbf{v}}_{\mathrm{m}} \\ \tilde{\mathbf{y}} \end{bmatrix}$.

As mentioned before, by the total reduction, $\mathbf{V}_k$ has the dimension $4n \times k$. Therefore, matrix $\mathbf{A}$ is modified by adding extra lines of zeros to adjust its size in the following form,

$$\mathbf{A}_{4n\times 4n} = \begin{bmatrix} a_{11} & a_{12} & \dots & a_{1n} \\ 0 & 0 & \dots & 0 \\ 0 & 0 & \dots & 0 \\ 0 & 0 & \dots & 0 \\ a_{21} & a_{22} & \dots & a_{2n} \\ 0 & 0 & \dots & 0 \\ 0 & 0 & \dots & 0 \\ 0 & 0 & \dots & 0 \\ \vdots & \vdots & \dots & \vdots \\ a_{n1} & a_{n2} & \dots & a_{nn} \\ 0 & 0 & \dots & 0 \\ 0 & 0 & \dots & 0 \\ 0 & 0 & \dots & 0 \end{bmatrix}.$$

However, the reduced system matrix $\tilde{\mathbf{A}} = \mathbf{V}_k^{\mathrm{T}}\mathbf{A}\mathbf{V}_k$ has the same dimension $k \times k$ for both partial and total reduction strategies and could be precomputed. $\mathbf{Bu}$ is also modified for the total reduction, accordingly. In Figure 3, we compare the two strategies for the errors of the transmembrane potential vs. runtime using a grid of 80 nodes. The relative L2-norm errors are computed with respect to the full order model (3) and averaged over the whole

[1] http://www.ians.uni-stuttgart.de/MoRePaS/software/kermor/

computational time. Using the total reduction rather than the partial reduction, more accurate solutions are achieved in smaller runtimes. Considering 30 modes for projecting $\mathbf{v}_m$, the error is four orders of magnitude smaller with a runtime of approximately 24 s. Therefore, we continue with the total reduction strategy for the following studies using the same grid and intervals of 5 modes for $\mathbf{v}_m$. In Figure 4, we show the errors of $\mathbf{v}_m$ vs. runtime and speedup for different grids. As expected the speedups become considerable for finer grids.

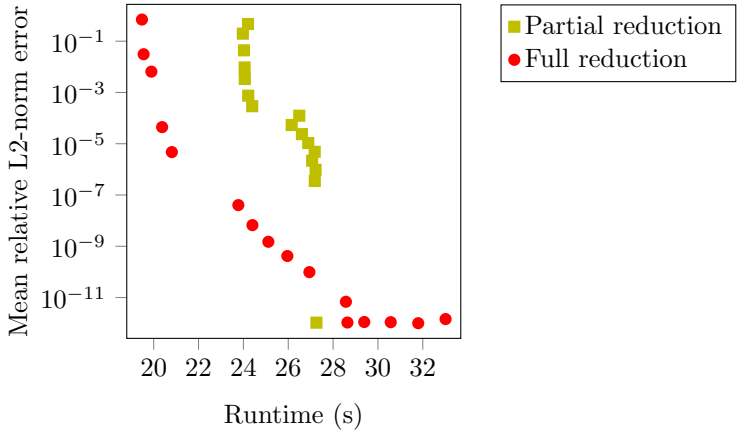

Figure 3: Comparison of the partial and total reduction strategies. Errors of the transmembrane potential with respect to the full order model are shown. A grid of 80 nodes is employed. Each point on the plot resembles 5 modes for the partial and 20 modes for total reduction (5 relevant modes for the transmembrane potential), respectively.

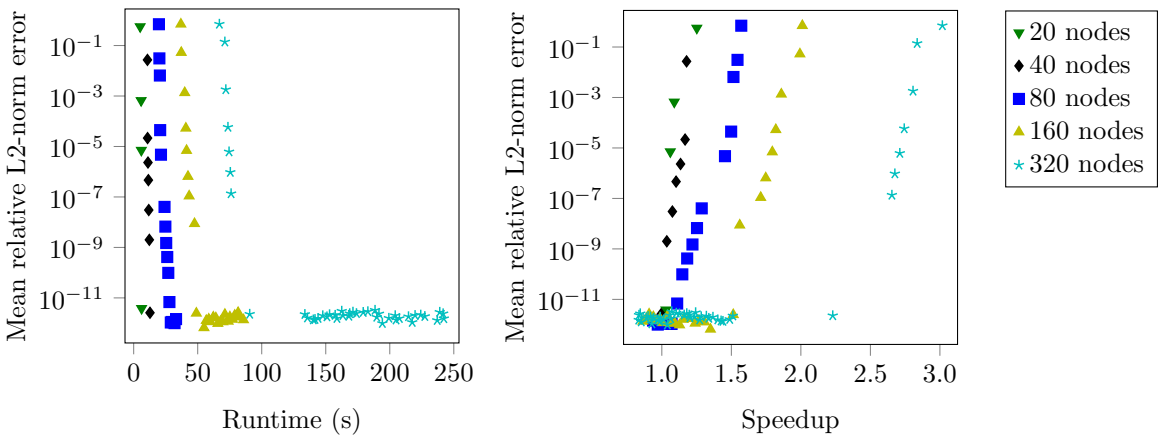

Figure 4: Errors of the transmembrane potential vs. runtime and speedup with respect to the full order model. The POD approach with the total reduction strategy is applied. A grid of 80 nodes is employed. Each point on the plot resembles 5 modes of the transmembrane potential.

6 POD-DEIM approach

Besides the total reduction strategy in equation (6a), we apply the discrete empirical interpolation method (DEIM) [9] to the nonlinear functions $\mathbf{F}$ and $\mathbf{G}$,

$$\begin{bmatrix} \tilde{\mathbf{v}}_{\mathrm{m}}^{*} \\ \tilde{\mathbf{y}}^{(n+1)} \end{bmatrix} = \begin{bmatrix} \tilde{\mathbf{v}}_{\mathrm{m}}^{(n)} \\ \tilde{\mathbf{y}}^{(n)} \end{bmatrix} + \mathbf{V}_k^{\mathrm{T}}\mathbf{U}_m(\mathbf{P}_m^{\mathrm{T}}\mathbf{U}_m)^{-1}\mathbf{P}_m^{\mathrm{T}} \begin{bmatrix} \mathbf{F}(\mathbf{v}_{\mathrm{m}}^{(n)}, \mathbf{y}^{(n)}) \\ \mathbf{G}(\mathbf{v}_{\mathrm{m}}^{(n)}, \mathbf{y}^{(n)}) \end{bmatrix} + \mathbf{V}_k^{\mathrm{T}}\mathbf{B}\mathbf{u}^{(n)}, \tag{7a}$$

$$\tilde{\mathbf{v}}_{\mathrm{m}}^{(n+1)} = \tilde{\mathbf{v}}_{\mathrm{m}}^{*} + \mathbf{V}_k^{\mathrm{T}}\mathbf{A}\mathbf{V}_k\tilde{\mathbf{v}}_{\mathrm{m}}^{(n+1)} \tag{7b}$$

where $\mathbf{U}_m, \mathbf{P}_m \in \mathbb{R}^{4n\times m}$ contain the projection basis and interpolation points, respectively. The basis $\mathbf{U}_m = [\mathbf{u}_1, ..., \mathbf{u}_m]$ is found by applying POD, where the SVD is performed on the snapshots,

$$\mathbf{H} = \begin{bmatrix} F_1^1 & F_1^2 & \dots & F_1^{n_s} \\ G_{11}^{\ 1} & G_{11}^{\ 2} & \dots & G_{11}^{\ n_s} \\ G_{21}^{\ 1} & G_{21}^{\ 2} & \dots & G_{21}^{\ n_s} \\ G_{31}^{\ 1} & G_{31}^{\ 2} & \dots & G_{31}^{\ n_s} \\ \vdots & \vdots & \dots & \vdots \\ F_n^1 & F_n^2 & \dots & F_n^{n_s} \\ G_{1_n}^{\ 1} & G_{1_n}^{\ 2} & \dots & G_{1_n}^{\ n_s} \\ G_{2_n}^{\ 1} & G_{2_n}^{\ 2} & \dots & G_{2_n}^{\ n_s} \\ G_{3_n}^{\ 1} & G_{3_n}^{\ 2} & \dots & G_{3_n}^{\ n_s} \end{bmatrix}.$$

The matrix $\mathbf{P}_m = [\mathbf{e}_{\wp_1}, ..., \mathbf{e}_{\wp_m}]$ contains columns of the identity matrix, where indices $\{\wp_1, ..., \wp_m\}$ are found through the DEIM algorithm with respect to the basis $\{\mathbf{u}_1, ..., \mathbf{u}_m\}$. Applying the above, the computational complexity of the nonlinear functions are independent of n. Because the functions must be evaluated only at the m interpolation

points, $\mathbf{P}_m^{\mathrm{T}} \begin{bmatrix} \mathbf{F} \\ \mathbf{G} \end{bmatrix} \in \mathbb{R}^{m\times 1}$. Therefore, the matrix vector multiplication of size $(k \times 4n)$ times $(4n \times 1)$ in equation (6a) is replaced by $(k \times m)$ times $(m \times 1)$. The matrix $\mathbf{V}_k^{\mathrm{T}}\mathbf{U}_m(\mathbf{P}_m^{\mathrm{T}}\mathbf{U}_m)^{-1} \in \mathbb{R}^{k\times m}$ is precomputed. We show the errors of the transmembrane potential vs. runtime for the POD-DEIM approach in Figure 6. A grid of 80 nodes is used as before. Each point on the plot resembles 20 POD modes (5 relevant modes for the transmembrane potential). $m/4n = 0.4, ..., 1$ is the ratio of the interpolation points. Using the DEIM approximation, the runtime could be reduced considerably for the same level of accuracy as expected. As one may also find out from the figure, the number of the DEIM interpolation points should be chosen equal or greater than number of the POD modes, $m \geq k$. The optimal number would be $m = k$ for the minimum runtime. A smaller number of interpolation points, would mean missing parts of the basis for the snapshots of the nonlinear functions, which are already included in the snapshots of the solution. According to our simulations, if $m < k$ while having less than 60 percent of the interpolation points, the solution is not stable when adding more POD modes by increasing k. If more than 60 percent of the points are used, the solution is stable but the error is not reduced further and is dominated by the error of the DEIM approximation. Our finding of the optimal choice is in agreement with [4], where they also found empirically the equal number of POD and DEIM modes as the best choice.

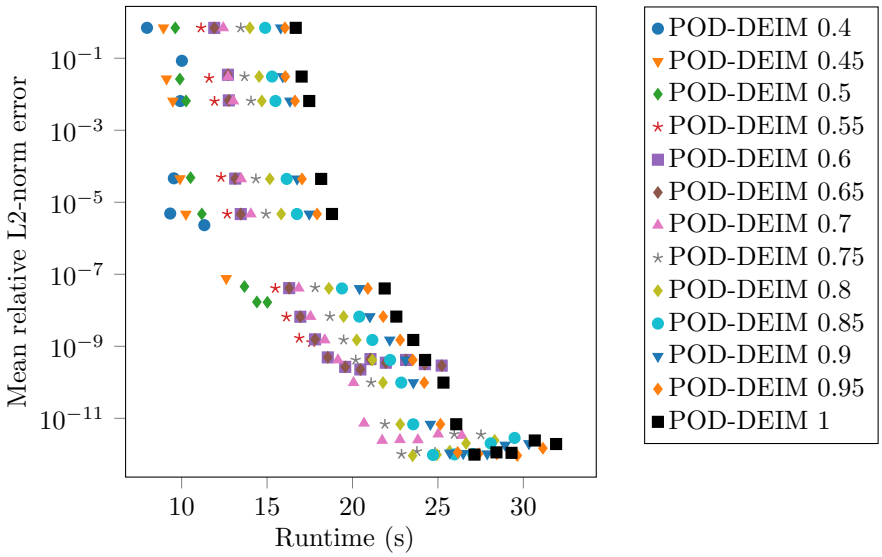

Figure 5: POD-DEIM approach for model order reduction. Errors of the transmembrane potential with respect to the full order model are shown. Ratios $m/4n$ for DEIM show the ratio of interpolation points used for evaluating the nonlinear functions. A grid of 80 nodes is employed. Each point on the plot resembles 20 modes (5 relevant modes for the transmembrane potential).

7 Conclusion and outlook

Due to the strong coupling between the transmembrane potential and ionic state variables, we propose a total reduction of them all together to build the POD basis. Comparing to the conventional partial reduction, where only the transmembrane potential is reduced, three ionic state variables resulting from the Hodgkin and Huxley (1952) model are additionally considered to build the snapshot matrix. The SVD decompositions of snapshot matrices using both reduction strategies show jumps in the singular values on different grids. However, using finer grids, the jumps disappear, which could be used as a sign for grid convergence. Considering a grid of 80 nodes and a threshold of 10^{-5} for the singular values, only 42 percent of the modes are above the threshold using the total reduction, while that would be 98 percent of the modes using the partial reduction. The effectiveness of the total reduction is approved by comparing the mean relative L2-norm errors of transmembrane potential for both strategies. Using 30 modes, the errors are four orders of magnitude smaller for the total reduction. To efficiently evaluate the nonlinear ionic current, we use the DEIM approximation. To adjust for the total reduction, the nonlinear functions corresponding to the state variables on the right-hand side of the nonlinear ODEs are approximated as well. Varying the number of DEIM interpolation points for a fixed number of POD modes could reduce the runtime for the same accuracy as expected. However, if the number of points is smaller than the modes, the solution is either unstable (using less than 60 percent of the points) or the errors are dominated by the DEIM approximation error. This could be understood as missing DEIM points because the snapshots of the nonlinear functions are present in and influence the snapshots of the solution. The equal number of DEIM points and POD modes appears to be the optimal choice, which is stable and accurate with considerably reduced runtime.
Our overall conclusion is that the potential for model order reduction lies mainly in reduction of the reaction term of the monodomain equation. This should be verified by considering more complicated models for chemical reactions such as the Shorten model [11], which contains more than 50 state variables.

8 Acknowledgments

This research was funded by the Baden-Württemberg Stiftung as part of the DiHu project of the High Performance Computing II program and the Cluster of Excellence for Simulation Technology (EXC 310/1).

REFERENCES

[1] O. Röhrle, J. B. Davidson, and A. J. Pullan. A physiologically based, multi-scale model of skeletal muscle structure and function. *Frontiers in Physiology*, 3, 2012.

[2] T. Heidlauf and O. Röhrle. Modeling the Chemoelectromechanical Behavior of Skeletal Muscle Using the Parallel Open-Source Software Library OpenCMISS. *Computational and Mathematical Methods in Medicine*, 2013:1–14, 2013.

[3] T. Heidlauf and O. Röhrle. A multiscale chemo-electro-mechanical skeletal muscle model to analyze muscle contraction and force generation for different muscle fiber arrangements. *Frontiers in Physiology*, 5(498):1–14, 2014.

[4] A. R. Kellems, S. Chaturantabut, D. C. Sorensen, and S. J. Cox. Morphologically accurate reduced order modeling of spiking neurons. *Journal of Computational Neuroscience*, 28(3):477494, 2010.

[5] A. L. Hodgkin and A. F. Huxley. A quantitative description of membrane current and its application to conduction and excitation in nerve. *The Journal of physiology*, 117(4):500–544, 1952.

[6] M. Boulakia, E. Schenone, and J-F. Gerbeau. Reduced-order modeling for cardiac electrophysiology. application to parameter identification. *International Journal for Numerical Methods in Biomedical Engineering*, 28(6-7):727–744, 2012.

[7] H. Yang and A. Veneziani. Efficient estimation of cardiac conductivities via POD-DEIM model order reduction. *Applied Numerical Mathematics*, 115:180 – 199, 2017.

[8] M. Mordhorst, T. Strecker, D. Wirtz, T. Heidlauf, and O. Rhrle. POD-DEIM reduction of computational EMG models. *Journal of Computational Science*, 19:86 – 96, 2017.

[9] S. Chaturantabut and D. C. Sorensen. Nonlinear model reduction via discrete empirical interpolation. *SIAM Journal on Scientific Computing*, 32(5):2737–2764, 2010.

[10] D. Wirtz. *Model Reduction for Nonlinear Systems: Kernel Methods and Error Estimation*. epubli GmbH, 2014.

[11] P. R. Shorten, P. O'Callaghan, J. B. Davidson, and T. K. Soboleva. A mathematical model of fatigue in skeletal muscle force contraction. *Journal of Muscle Research and Cell Motility*, 28(6):293–313, 2007.